Experimental study of the $3^3\Pi_g$ and $4^3\Sigma_g^+$ states of the rubidium dimer

P. T. Arndt,[1] V. B. Sovkov,[2,3] J. Ma,[3,4] X. Pan,[1] D. S. Beecher,[1] J. Y. Tsai,[1] R. Livingston,[1] V. M. Marcune,[1] A. M. Lyyra,[1] and E. H. Ahmed[1,*]

[1]*Physics Department, Temple University, Philadelphia, Pennsylvania 19122, USA*

[2]*Saint Petersburg State University, 7/9 Universitetskaya naberezhnaya, Saint Petersburg 199034, Russia*

[3]*State Key Laboratory of Quantum Optics and Quantum Optics Devices, Institute of Laser Spectroscopy, College of Physics and Electronics, Shanxi University, Taiyuan 030006, China*

[4]*Collaborative Innovation Center of Extreme Optics Shanxi University Taiyuan, Shanxi 030006, People's Republic of China*

(Received 18 October 2021; accepted 7 March 2022; published 31 March 2022)

This paper reports a high-resolution experimental study of the $3^3\Pi_g$ and $4^3\Sigma_g^+$ electronic states of the $^{85}Rb_2$ dimer. In the experiment, rovibrational levels of the two electronic states were probed using the perturbation facilitated optical-optical double resonance technique by exciting $^{85}Rb_2$ molecules from thermally populated levels of the ground $X^1\Sigma_g^+$ state through intermediate levels of the mixed $A^1\Sigma_u^+ \sim b^3\Pi_u$ electronic states. The resonances of the probe laser were observed by detecting the laser induced fluorescence from the target states to the $a^3\Sigma_u^+$ triplet ground state. In addition, to confirm the triplet character as well as the vibrational quantum number assignment of the states, for selected resonances the fluorescence to the $a^3\Sigma_u^+$ state was resolved and bound-free spectra were recorded. From the observed term values for each state potential-energy curves were constructed using the Rydberg-Klein-Rees method.

DOI: 10.1103/PhysRevA.105.032823

I. INTRODUCTION

Interatomic potentials of alkali-metal dimers are of fundamental importance for the understanding and description, among other things, of the formation of ultracold ground-state molecules, Bose-Einstein and Fermi condensates, and ultracold atom-molecule collisions Refs. [1–8]. From the homonuclear alkali-metal dimers the lighter Li_2 [9–23] and Na_2 [20,24–33] molecules have been studied in most detail. A number of studies have been also devoted to the heavier K_2 dimer [34–44]. The electronic structures of the heaviest homonuclear alkali-metal dimers Rb_2 [45–57] and Cs_2 [58–65] are less well known due to experimental difficulties associated with the relatively large densities of states as well as the presence of strong perturbations and character mixing arising from effects such as the spin-orbit interaction. There are a number of *ab initio* studies of the Rb_2 dimer [66–76] and even though the accuracy of such calculations has improved significantly, they are not yet suitable for direct use in experiments relying on precise knowledge of the energy of levels and transitions. Thus, experimental results on the electronic structure of the Rb_2 molecule are still highly desirable. The singlet and triplet, $X^1\Sigma_g^+$ [48,49] and $a^3\Sigma_u^+$ [51], ground states of the Rb_2 dimer as well as the electronic states arising from the first excited atomic limit ($5s + 5p$) such as the $A^1\Sigma_u^+ \sim b^3\Pi_u$ [48,50,53] and the $B^1\Pi_u$ [47] states are well described experimentally with high accuracy. In contrast, there are only limited experimental data for the electronic states of the rubidium dimer arising from higher atomic limits. Recently we have reported experimental observations of the singlet $3^1\Pi_g$ and $6^1\Sigma_g^+$ electronic states of the Rb_2 molecule [77,78]. Building on these results in this paper we extend our spectroscopic studies to the triplet $3^3\Pi_g$ and $4^3\Sigma_g^+$ states present in the same energy range 24 000−26 000 cm^{-1}.

II. EXPERIMENT

The experimental setup is shown in Fig. 1. It is similar to the setup used previously to study the $3^1\Pi_g$ and $6^1\Sigma_g^+$ electronic states of the Rb_2 molecule [77,78]. Briefly, rubidium metal (Alfa Aesar 10315, 99.75%) with a natural abundance ratio of the ^{85}Rb (72.17%) and ^{87}Rb (27.83%) isotopes [79] was loaded into a heat-pipe oven. Only transitions of the $^{85}Rb_2$ isotopologue of the rubidium dimer were probed in this experiment. To contain the rubidium vapor in the center of the heat-pipe oven [80] argon (Airgas UHP300, 99.999%) was used as a buffer gas at 2-Torr pressure (room temperature). The center of the heat-pipe oven was heated with electric heaters to a temperature of 180 °C producing the Rb_2 dimer at a pressure of approximately 1.8×10^{-5} Torr [81]. From the temperature of the oven we estimate a Doppler linewidth (full width at half maximum) for the pump transition of about 400 MHz [82].

Counterpropagating laser beams in a cascade pump-probe configuration were employed to study the 24 000–26 000 cm^{-1} energy region as illustrated in Fig. 2. The pump laser excited the molecules from thermally populated rovibrational levels of the ground $X^1\Sigma_g^+$ electronic state to an intermediate level from the $A^1\Sigma_u^+ \sim b^3\Pi_u$ states manifold. The $A^1\Sigma_u^+$ and $b^3\Pi_u$ states strongly perturb each other due

*Corresponding author: erahmed@temple.edu

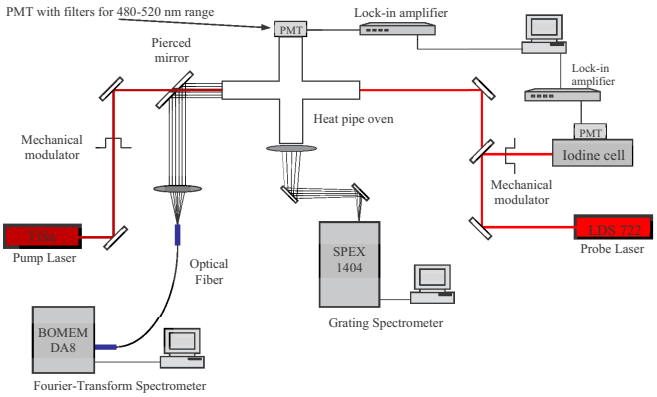

FIG. 1. Schematic diagram of the experimental setup. Tunable cw single-mode narrow-band (≈1 MHz) Coherent 899-29 titanium sapphire (L_{pump}) and Coherent 699-29 with LDS 722 dye (L_{probe}) lasers are used as the pump and probe, respectively. L_{pump} and L_{probe} are in the counterpropagating configuration. Probe laser resonances to the $3^3\Pi_g$ and $4^3\Sigma_g^+$ states are observed by monitoring LIF to the $a^3\Sigma_u^+$ state with a photomultiplier tube (R928P Hamamatsu Photonics) detector attached to one of the side arms of the heat-pipe oven. The bound-free fluorescence from the $3^3\Pi_g$ and $4^3\Sigma_g^+$ states was recorded using a SPEX 1404 grating spectrometer with a photomultiplier tube (R928P Hamamatsu Photonics) detector.

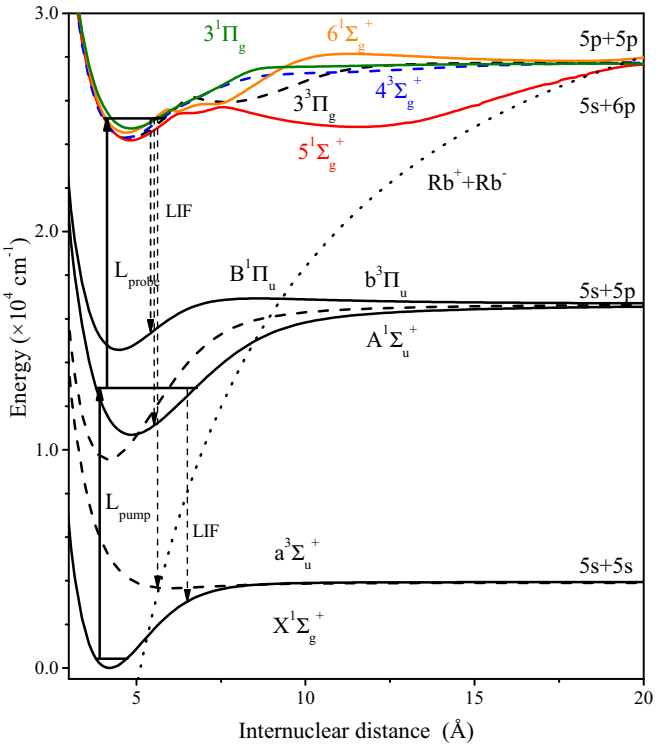

FIG. 2. Excitation scheme of the experiment and potential-energy curves of the rubidium dimer. The pump laser excites molecules from a single thermally populated rovibrational level of the $X^1\Sigma_g^+$ ground electronic state to an intermediate level with a mixed multiplicity character from the $A^1\Sigma_u^+ \sim b^3\Pi_u$ manifold. The probe laser further excites these molecules to the target $3^3\Pi_g$ and $4^3\Sigma_g^+$ electronic states. The probe laser resonances are detected by monitoring the fluorescence from the $3^3\Pi_g$ and $4^3\Sigma_g^+$ states to the $a^3\Sigma_u^+$ state. The potential curves used in the figure are *ab initio* calculations from Ref. [76]. The dotted curve is the $Rb^+ + Rb^-$ Coulomb potential energy $e^2/(4\pi\varepsilon_0 R)$.

to their substantial spin-orbit coupling, inherited from the $5p$ atomic state with fine-structure splitting of its $^2P_{1/2}$ and $^2P_{3/2}$ doublet of 237.595 cm^{-1} [83]. Thus, the rovibrational levels of the $A^1\Sigma_u^+ \sim b^3\Pi_u$ manifold have a mixture of singlet and triplet multiplicity. This allowed us to access the triplet exited states of the rubidium molecule using the perturbation facilitated optical-optical double resonance (PFOODR) technique [13,25,84] starting from levels of the $X^1\Sigma_g^+$ ground electronic state with pure singlet character. All intermediate levels from the $A^1\Sigma_u^+ \sim b^3\Pi_u$ manifold used in the experiment nominally belong to the $A^1\Sigma_u^+$ state; the singlet multiplicity character is the dominant component, with substantial admixture exclusively from the $b^3\Pi_{0u}$ component only.

Resolved laser induced fluorescence (LIF) spectra from the intermediate levels to the ground $X^1\Sigma_g^+$ state were recorded with a Fourier-transform infrared spectrometer (FTIR, Bomem DA8) at a resolution of 0.01 cm^{-1}. The FTIR spectrometer was calibrated with a uranium hollow cathode lamp [85,86]. Excitation of a specific intermediate level was confirmed by observing matching *PR* progressions in the resolved fluorescence spectra of the *P* and *R* branch $A^1\Sigma_u^+ - X^1\Sigma_g^+$ pump laser transitions. An example for such spectra is given in Fig. 3 for the $A^1\Sigma_u^+ \sim b^3\Pi_u(n' = 148, J = 30)$ intermediate level. In addition, the observed LIF resonances were matched with transition frequency predictions from the term values of the $X^1\Sigma_g^+$ [49] and $A^1\Sigma_u^+ \sim b^3\Pi_u$ [50] states. The label n' (not a quantum number), adopted from Ref. [50], denotes the coupled-channel vibrational eigenstates by increasing energy of the $A^1\Sigma_u^+$ and $b^3\Pi_u$ mixed electronic states. For the angular momenta and their projections on the molecular axis we follow standard notations [87]; $\vec{S}$ total electron spin with projection Σ, $\vec{L}$ electron orbital angular momentum with projection Λ, $\vec{R}$ nuclear rotational angular momentum, $\vec{J} = \vec{R} + \vec{S} + \vec{L}$ total orbital angular momentum excluding nuclear spin with projection $\Omega = \Sigma + \Lambda$, and $\vec{N} = \vec{R} + \vec{L}$ with projection Λ.

The resonances to the $3^3\Pi_g$ and $4^3\Sigma_g^+$ states were observed by detecting LIF emission to the $a^3\Sigma_u^+$ state in the 480–520-nm range using a photomultiplier tube (PMT, R928P Hamamatsu Photonics) attached to one of the side arms of the heat pipe. Color filters (Kopp Glass 4303 and 4305) were used to suppress the amount of laser scatter and fluorescence outside of the wavelength range of interest reaching the PMT. The current output of the PMT was amplified with a lock-in amplifier (SR850 Stanford Research) while the pump laser beam was repetitively switched on and off at a frequency of approximately 1 kHz using a rotating chopper (SR540 Stanford Research). The probe laser was scanned continuously in the energy range 13 300–14 000 cm^{-1}, calibrated using the iodine atlas [88,89] in a similar fashion as described in Ref. [77], while the amplified output of the PMT detector was recorded as a function of the laser frequency. The iodine signal was amplified using a lock-in amplifier (SR850) in the same fashion as the LIF signal. A large number of resonances, with many of them accidental, were

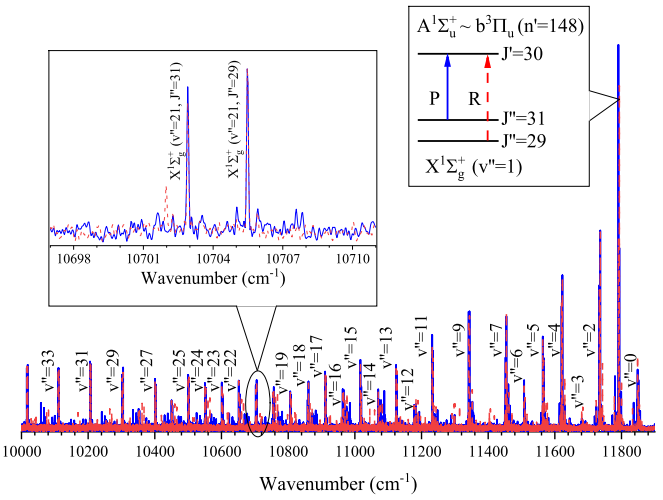

FIG. 3. Resolved LIF spectra from the $A^1\Sigma_u^+ \sim b^3\Pi_u(n' = 148, J' = 30)$ intermediate level used to confirm the pump laser P and R branch resonances. The spectra are recorded with a BOMEM DA8 FTIR spectrometer. In the main panel and the inset the fluorescences from the $A^1\Sigma_u^+ \sim b^3\Pi_u(n' = 148, J' = 30) \leftarrow X^1\Sigma_g^+(v'' = 1, J'' = 31)$ and $A^1\Sigma_u^+ \sim b^3\Pi_u(n' = 148, J' = 30) \leftarrow X^1\Sigma_g^+(v'' = 1, J'' = 29)$ pump excitations are indicated with solid blue and dashed red lines, respectively.

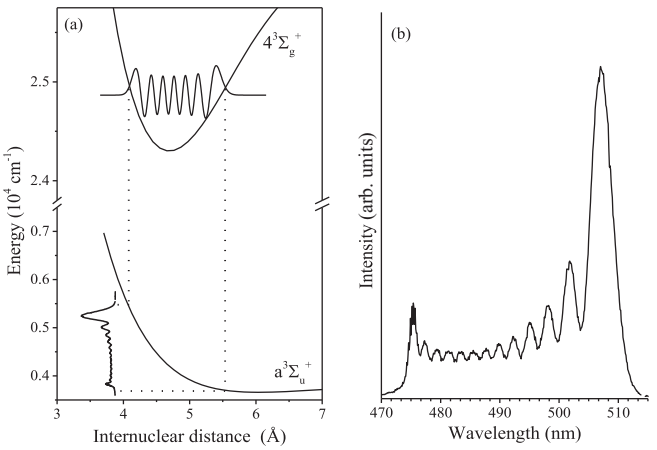

FIG. 4. Example bound-free spectrum from $v = 12$ of the $4^3\Sigma_g^+$ electronic state to the repulsive region of the $a^3\Sigma_u^+$ state potential. (a) The intensity of bound-free emission from a bound level to a repulsive potential on which the molecule dissociates into two free atoms is proportional to the probability distribution of the excited-state wave function [90]. The energy range of the spectrum is determined by the term energy of the emitting level and the potential-energy curve of the lower electronic state. (b) Experimentally recorded bound-free spectrum from the $4^3\Sigma_g^+(v = 12, J = 11)$ level.

observed in each probe laser scan due to the high density of rovibrational levels of the rubidium molecule. To distinguish the probe laser resonances originating from the specific target $A^1\Sigma_u^+ \sim b^3\Pi_u(n', J')$ intermediate level from all other resonances, each probe laser scan was acquired twice with the pump laser at $A^1\Sigma_u^+ \sim b^3\Pi_u(n', J') \leftarrow X^1\Sigma_g^+(v'', J' + 1)$ and $A^1\Sigma_u^+ \sim b^3\Pi_u(n', J') \leftarrow X^1\Sigma_g^+(v'', J' - 1)$ transitions, respectively. Only the probe laser resonances observed at the same frequency with similar intensity and line shape for both pump branches were considered as originating from the $A^1\Sigma_u^+ \sim b^3\Pi_u(n', J')$ intermediate level.

In the probe laser scans vibrational progressions of two electronic states were observed with each vibrational transition containing P and R rotational branches. From the mixed $A^1\Sigma_u^+ \sim b^3\Pi_u$ intermediate levels excitations to singlet as well as triplet states are possible. To determine the electron-spin multiplicity of the excited states, bound-free fluorescence [90] from selected rovibrational levels to the repulsive part of the $a^3\Sigma_u^+$ state potential was recorded at a resolution of ≈ 0.75 nm using a SPEX 1404 grating spectrometer with fully open (3-mm-width) slits. The LIF from the side arm of the heat pipe was directed, with the aid of a set of mirrors and lenses, to the entrance slit of the spectrometer. The spectra were recorded by scanning the spectrometer while the pump and probe laser were held on resonance. An example spectrum illustrating the structure and origin of the observed bound-free fluorescence is given in Fig. 4. Well-developed oscillatory fluorescence features [90,91] were observed in the recorded spectra of the $3^3\Pi_g$ and $4^3\Sigma_g^+$ states (see Fig. 5), a clear indication of a triplet spin multiplicity. In contrast, this is not the case for singlet states since the transitions to the $a^3\Sigma_u^+$ state are not directly allowed and instead the bound-free fluorescence arises due to coupling and collisional transfer with nearby excited triplet states. An additional important application of the observed bound-free spectra was their use in assignment of the vibrational quantum number for the observed levels by counting the nodes [90] present in each spectrum.

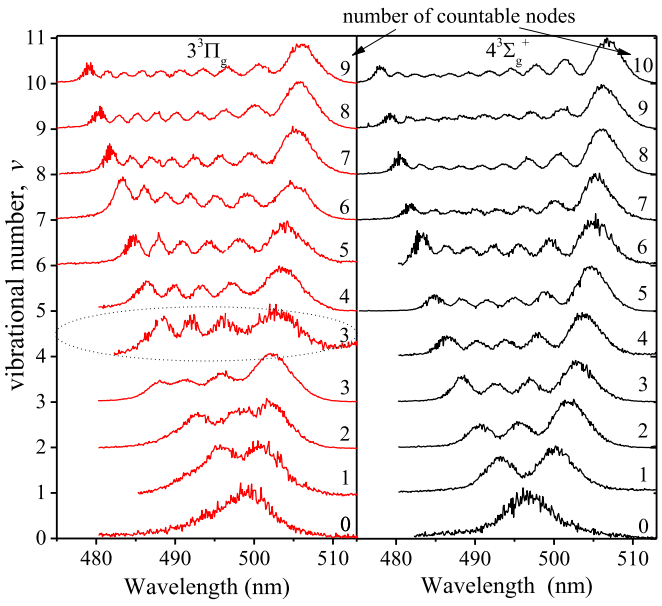

FIG. 5. The resolved bound-free emission for the first 11 vibrational levels of the $3^3\Pi_g$ (left) and the $4^3\Sigma_g^+$ (right) electronic states. The bound-free spectra for the remaining observed vibrational levels are included in the Supplemental Material [98]. The number of countable nodes is indicated on the left side of each spectrum. The bound-free spectrum ($v = 4$) of the $3^3\Pi_g$ state showing the onset of the vanishing node is highlighted with a dotted oval.

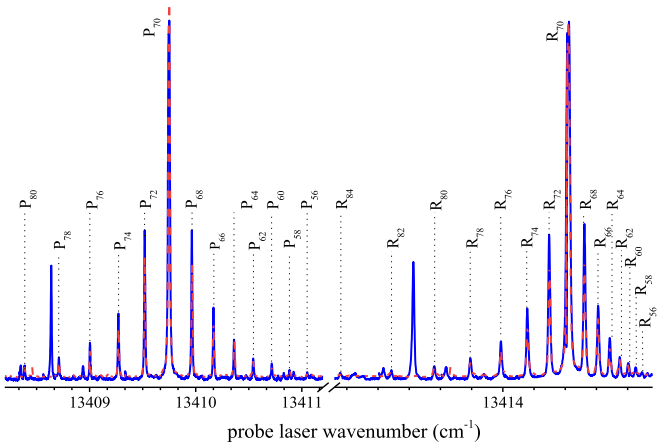

FIG. 6. A probe laser excitation spectrum of the $4^3\Sigma_g^+(v = 11)$ vibrational level from the $A^1\Sigma_u^+ \sim b^3\Pi_u(n' = 106,\ J' = 70)$ intermediate level. In addition to the main (parent) P_{70} and R_{70} lines, satellite lines due to collision-induced ΔJ even rotational energy transfer (RET) in the intermediate level are observed. The solid (blue) and dashed (red) traces correspond to a pump laser resonant with the P_{71} and R_{69} excitations to the $A^1\Sigma_u^+ \sim b^3\Pi_u(n' = 106,\ J' = 70)$ intermediate level from the $X^1\Sigma_g^+(v'' = 0)$ ground-state vibrational level, respectively.

Using *ab initio* predictions [76] in conjunction with the electronic and rotational transition selection rules for diatomic molecules [92] applied to the triplet $b^3\Pi_{0u}$ component of the mixed intermediate levels, the two observed states were identified as the $3^3\Pi_g$ and $4^3\Sigma_g^+$ electronic states. A good representation for the $^3\Pi$ states of Rb_2 is Hund's case (a) [93]. Thus, on account of the $\Delta\Sigma = 0$ selection rule the probe transitions observed for the $3^3\Pi_g$ state must be to its $\Omega = 0$ ($\Delta\Omega = \Delta\Sigma + \Delta\Lambda = 0$) component ($3^3\Pi_{0g} \leftarrow A^1\Sigma_u^+ \sim b^3\Pi_{0u}$). This is further corroborated by the absence of weak Q branch transitions in our spectra. In Hund's case (a) $^3\Pi_0 \leftarrow {}^3\Pi_0$ transitions have only P and R branches, while $^3\Pi_1 \leftarrow {}^3\Pi_1$ and $^3\Pi_2 \leftarrow {}^3\Pi_2$ transitions in addition exhibit a weak Q branch [92].

In addition to the direct probe laser resonances, a number of collisional satellites (see Fig. 6) as described in previous experiments in heat-pipe ovens [94–96] were observed. In our case the satellite lines occur because of inelastic J changing collisions between Rb_2 molecules excited to the intermediate level and argon or rubidium atoms present in the heat pipe. A spectrum observed due to collisionally induced transfer between levels, in general, is a result of an ensemble average of binary collisions with statistical distribution of parameters such as the relative collision velocity and initial orientation of the colliding partners. Thus, the rules for transitions between levels of a molecule arising from collisions with other atoms or molecules lack the rigor of radiative transitions. Nevertheless, by considering the symmetry of the initial and final states, propensity rules often can be obtained. In the discussion below we derive the propensity rule for the J-changing collisions observed in our experiment by following the general analysis given in Refs. [87,92]. The ^{85}Rb nuclei are fermions with a nuclear spin of 5/2. Therefore, the total molecular wave function ψ_{total} of the $^{85}Rb_2$ molecule must be antisymmetric (Pauli exclusion principle) under the action of the nuclei exchange operator P_{12}, i.e., $P_{12}\psi_{\text{total}} = -\psi_{\text{total}}$. In most cases it is possible to write $\psi_{\text{total}} = \psi\psi_{\text{ns}}$, where ψ_{ns} is the nuclear-spin component of the total wave function and ψ contains all other, such as electron-spin, orbital, vibrational, and rotational, components. The possible values of the total nuclear spin, I, for the $^{85}Rb_2$ molecule are 5, 4, 3, 2, 1, and 0. The *ortho* nuclear-spin configurations ($I = 5$, 3, 1 and statistical weight $g = 21$) have symmetric ψ_{ns} functions, while the *para* nuclear-spin configurations ($I = 4$, 2, 0 and statistical weight $g = 15$) have antisymmetric ψ_{ns} functions. When we consider P_{12} acting only on ψ we have $P_{12}\psi = \pm\psi$, where the symmetric positive states are labeled as s and the antisymmetric negative states are labeled as a. The symmetry of the rotational levels of the $A^1\Sigma_u^+$ state, the dominant character of the intermediate levels used in the experiment, alternate with J (even J levels have a symmetry and odd J levels have s symmetry) [87]. Therefore, for ψ_{total} to be antisymmetric the rotational levels of the $A^1\Sigma_u^+$ state with a symmetry (even J) must be associated with *ortho* nuclear-spin states and conversely s symmetry rotational levels (odd J levels) must be associated with *para* nuclear-spin configurations. Selection rules stipulate that the total symmetry (parity) of the molecule must be rigorously preserved during transitions, including transitions arising from collisions. Collisions that change the nuclear-spin symmetry are rare [92,97], indicating that the symmetry of ψ is preserved during most collisions. Therefore, during collisions a propensity for symmetric-symmetric ($s \leftrightarrow s$) and antisymmetric-antisymmetric ($a \leftrightarrow a$) transfer exists while transfer between symmetric and antisymmetric states ($s \nleftrightarrow a$) is strongly suppressed (see p. 131 of Ref. [92]). From this follows that only even J changing collisional satellite lines, $\Delta J = \pm 2, \pm 4, \ldots$, will be observed in the experiment. The collisional lines enhance the rotational data acquired for each observed vibrational level of the two electronic states. The steps in the procedure of assigning their rotational quantum numbers are discussed in detail in Ref. [78].

III. RESULTS AND ANALYSIS

The $3^3\Pi_g$ and $4^3\Sigma_g^+$ states of the Rb_2 molecule lie in an energy region with a high density of electronic states (see Fig. 2) as predicted by *ab initio* calculations [75,76] and previous experimental observations [77,78]. The interactions between the electronic states of *gerade* symmetry $3^1\Pi_g$, $5^1\Sigma_g^+$, $6^1\Sigma_g^+$, $3^3\Pi_g$, and $4^3\Sigma_g^+$ in this range cause perturbations of their rovibrational levels. In addition, *ab initio* predictions indicate especially strong interactions between these states around 26 000 cm^{-1} which become evident by the unusual features such as avoided crossings and secondary wells present in their adiabatic potential curves. Nevertheless, in our experimental observations we were able to discern two vibrational progressions which we have assigned to the $3^3\Pi_g$ and $4^3\Sigma_g^+$ electronic states. The rovibrational energy data observed in the experiments for the $3^3\Pi_g$ and $4^3\Sigma_g^+$ states are illustrated in Fig. 7. The rotational quantum numbers in the plots, J for the $3^3\Pi_g$ state (Hund's case (a)) and N for the $4^3\Sigma_g^+$ state (Hund's case (b)), were derived from the rotational quantum number of the intermediate level $A^1\Sigma_u^+ \sim b^3\Pi_u(n', J')$ for the P and R probe laser excitation branches as J (or N) $= J' - 1$ and

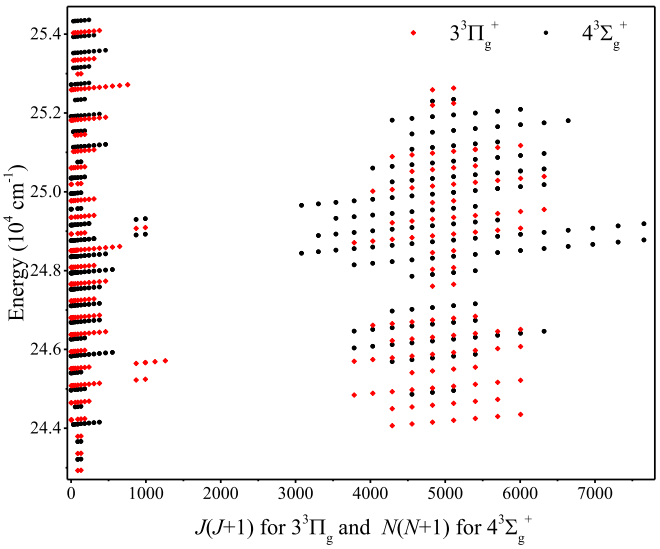

FIG. 7. The observed rovibrational levels of the (a) $3^3\Pi_g$ and the (b) $4^3\Sigma_g^+$ electronic states. For the $3^3\Pi_g$ state, 400 rovibrational levels, spanning the range of the vibrational quantum number $v = 0$ through 27 and the rotational quantum number $J = 0$ through 79. A total of 506 rovibrational levels in a similar range of vibrational and rotational quantum numbers were observed for the $4^3\Sigma_g^+$ state.

$J' + 1$, respectively. The term energy of each of the observed levels along with details of the excitation pathways used to access them are given in the Supplemental Material [98].

The vibrational quantum number is typically very difficult to obtain in this type of spectroscopic study due to the lack of selection rules for vibrational transitions. Nevertheless, in this case we were able to create assignment for the vibrational quantum numbers of the observed levels from the experimentally measured bound-free spectra presented in Fig. 5. An unusual behavior in the bound-free spectra is observed going from $v = 3$ to 4 for the $3^3\Pi_g$ state (see Fig. 5) where one of the nodes vanishes and the node count for the vibrational levels with $v \geqslant 4$ is $v-1$. Similarly, a node vanishes in the bound-free spectra of the $4^3\Sigma_g^+$ state going from $v = 16$ to 17. There are several possible causes for such puzzling behavior, but none appear to give satisfactory explanation. For example, if a shelf or second minimum develops in the potential curve, it will strongly affect the bound-free spectrum due to an onset of sampling at longer R range of the upper state rovibrational wave function. We believe this is not likely in our case since the observed vibrational spacing is not consistent with the shelf or second minimum region. Moreover, these features are not present in the corresponding energy range of either the *ab initio* curves of Ref. [76] or the experimental potential curves derived in this paper. Another possible cause is a rapid decrease in the electronic transition dipole moment function of the upper states with the $a^3\Sigma_u^+$ state in a relatively narrow R range near R_e, where the large momentum of the molecules results in closely spaced nodes. Then, the combination of low amplitude and close spacing can lead to unresolved nodes in the experimental bound-free spectra. Unfortunately, we cannot further explore this possibility since the transition dipole moment functions of the $3^3\Pi_g$ and $4^3\Sigma_g^+$ states with the $a^3\Sigma_u^+$ state are not known. In addition, no obvious low intensity range in the bound-free spectra is observed. A third alternative is an interference effect due to borrowed oscillator strength from another triplet state that has an allowed transition to the $a^3\Sigma_u^+$ state. The drawback of this hypothesis is that no additional triplet states were observed in our experiments.

The calculations described below were carried out using the computational package OPTIMIZER [99]. The main package, along with the library of application programs for quantum-mechanical simulations and analysis of molecular spectra, is freely available for download [100]. The project OPTIMIZER is continually being developed and expanded. In this context, we would like to mention that many of our previous analyses of alkali-metal dimers also used OPTIMIZER [39,40,43,51,59,61,64,77,78,101–103].

Following the assignments of the vibrational and rotational quantum numbers of the observed term values the data for the $3^3\Pi_g$ and $4^3\Sigma_g^+$ states were fitted by a least-squares method with

$$T_{v,J} = \sum_{k,l} Y_{k,l}(v + 1/2)^k [\, J(\, J + 1) - \Omega^2 + S(S + 1) - \Sigma^2]^l \tag{1a}$$

and

$$T_{v,J} = \sum_{k,l} Y_{k,l}(v + 1/2)^k [\, N(N + 1) - \Lambda^2]^l, \tag{1b}$$

the Dunham expansion [104] equations for Hund's cases (a) and (b) [92], respectively. A series of fits in which a balance between improvements in the fits and statistical significance of newly added constants were carried out to determine the optimum set of coefficients for each state. Considering that all the experimental results were acquired under the same conditions, equal weights were used for all data points in the fitting process. The final results of the fitting process for both states are presented in Table I. Once the Dunham coefficients were determined, the potential-energy curves of the states were generated by utilizing the first-order semiclassical Rydberg-Klein-Rees (RKR) method [105–108]. The results for the turning points $R_{\min}$ and $R_{\max}$ of the potentials together with the $G_v + Y_{0,0} = \sum_k Y_{k,0}(v + 1/2)^k$ values (i.e., the values of the potential-energy functions relative to their minima) are tabulated in Tables II and III for the $3^3\Pi_g$ and $4^3\Sigma_g^+$ states. The tables include the effective vibrational quantum numbers at the bottoms of the potential wells, $v = -0.5001$ and -0.4959 for the $3^3\Pi_g$ and $4^3\Sigma_g^+$ states, respectively. Their difference from $-1/2$ indicates that the Kaiser correction [109,110] was embedded into the RKR algorithm. The RKR and *ab initio* potentials [76] for both states are plotted in Fig. 8.

Our experimental values for the molecular constants, T_e, ω_e, and B_e, are generally in line with the *ab initio* predictions as illustrated in Table IV. Nevertheless, it should be noted that the experimental B_e values are consistently smaller than the *ab initio* predictions. This is reflected in Fig. 8 where the experimental potentials are shifted to larger internuclear distance relative to the theoretical curves from Ref. [76]. We note that at the equilibrium internuclear distance of a molecular potential R_e and B_e are related according to the

TABLE I. Dunham expansion coefficients (in cm^{-1}) of the $3^3\Pi_g$ and the $4^3\Sigma_g^+$ electronic states of Rb_2 obtained by direct fit of the experimental data. The last two rows represent the estimates based on the approximate correlations [104,109,111–113]: $Y'_{00} \cong \frac{Y_{01}+Y_{20}}{4} - \frac{Y_{11}Y_{10}}{12Y_{01}} + \frac{Y_{11}^2Y_{10}^2}{144Y_{01}^3}$ and $Y'_{02} \cong -4\frac{Y_{01}^3}{Y_{10}^2}$.

k, l	$Y_{k,l}$ for $3^3\Pi_g$	$Y_{k,l}$ for $4^3\Sigma_g^+$
$T_e + Y_{00}$	24268.409 (138)	24294.789 (349)
Y_{10}	44.2151 (561)	47.6712 (2628)
Y_{20}	$-1.6451\,(742) \times 10^{-1}$	-1.04188 (6954)
Y_{30}	$1.0336\,(380) \times 10^{-2}$	$1.30715\,(8489) \times 10^{-1}$
Y_{40}	$-3.0025\,(655) \times 10^{-4}$	$-9.42103\,(52195) \times 10^{-3}$
Y_{50}		$3.16996\,(1569) \times 10^{-4}$
Y_{60}		$-3.93547\,(18310) \times 10^{-6}$
Y_{01}	$1.6767\,(62) \times 10^{-2}$	$1.7335\,(59) \times 10^{-2}$
Y_{11}	$-8.79\,(138) \times 10^{-5}$	$-1.101\,(90) \times 10^{-4}$
Y_{21}	$8.17\,(144) \times 10^{-6}$	$2.50\,(37) \times 10^{-6}$
Y_{31}	$-2.730\,(445) \times 10^{-7}$	
Y_{02}	$1.79\,(88) \times 10^{-8}$	$-9.6\,(71) \times 10^{-9}$
Y'_{00}	0.0046 (90)	-0.1942 (191)
Y'_{02}	$-9.64\,(10) \times 10^{-9}$	$-9.17\,(15) \times 10^{-9}$

TABLE II. RKR potential of the $3^3\Pi_g$ state generated from the Dunham coefficients listed in Table I.

v	$R_{\min}$(Å)	$R_{\max}$(Å)	$G_v + Y_{00}(cm^{-1})$
−0.5001	$R_e = 4.866349\,(898)$ Å		0
0	4.738071	5.006532	22.072
1	4.650265	5.116445	65.990
2	4.591769	5.194927	109.664
3	4.544887	5.259856	153.140
4	4.504562	5.316479	196.460
5	4.468538	5.367252	239.656
6	4.435601	5.413597	282.755
7	4.405025	5.456452	325.775
8	4.376345	5.496502	368.727
9	4.349252	5.534280	411.617
10	4.323532	5.570225	454.442
11	4.299039	5.604717	497.190
12	4.275666	5.638097	539.846
13	4.253341	5.670675	582.385
14	4.232012	5.702747	624.774
15	4.211645	5.734596	666.975
16	4.192216	5.766498	708.943
17	4.173712	5.798730	750.623
18	4.156126	5.831570	791.955
19	4.139455	5.865302	832.872
20	4.123703	5.900224	873.299
21	4.108872	5.936648	913.153
22	4.094968	5.974909	952.346
23	4.081996	6.015372	990.780
24	4.069959	6.058439	1028.350
25	4.058861	6.104561	1064.952
26	4.048697	6.154252	1100.460
27	4.039458	6.208112	1134.752

TABLE III. RKR potential of the $4^3\Sigma_g^+$ state generated from the Dunham coefficients listed in Table I.

V	$R_{\min}$(Å)	$R_{\max}$(Å)	$G_v + Y_{00}(cm^{-1})$
−0.4959	$R_e = 4.786005\,(821)$ Å		0
0	4.663113	4.922381	23.397
1	4.578073	5.034438	69.364
2	4.521998	5.117130	114.177
3	4.478086	5.187118	158.242
4	4.441418	5.249235	201.829
5	4.409624	5.305817	245.094
6	4.381277	5.358289	288.111
7	4.355416	5.407634	330.893
8	4.331351	5.454572	373.413
9	4.308582	5.499631	415.625
10	4.286750	5.543191	457.475
11	4.265611	5.585505	498.919
12	4.245012	5.626713	539.925
13	4.224884	5.666854	580.490
14	4.205220	5.705882	620.635
15	4.186067	5.743680	660.410
16	4.167503	5.780082	699.893
17	4.149624	5.814900	739.185
18	4.132515	5.847962	778.401
19	4.116229	5.879141	817.662
20	4.100763	5.908401	857.082
21	4.086036	5.935830	896.751
22	4.071867	5.961673	936.714
23	4.057960	5.986365	976.958
24	4.043879	6.010559	1017.378
25	4.029025	6.035182	1057.754
26	4.012580	6.061510	1097.722
27	3.993417	6.091331	1136.741

following equation [87]:

$$B_e = \frac{h \times 10^{-2}}{8\pi^2 \mu c} \times \frac{1}{R_e^2}, \tag{2}$$

where B_e is in cm^{-1} units while all physical constants are in SI units. The reduced mass of the $^{85}Rb_2$ molecule is $\mu = m(^{85}Rb)/2 = 7.04\,997\,97\,224 \times 10^{-26}$ kg (42.45 58 962 amu) [79]. The systematic discrepancy in R illustrated in Fig. 8 is possibly an indication of incompletely or incorrectly accounted couplings in the *ab initio* calculations. This is further corroborated by the discrepancy between the *ab initio* and

TABLE IV. Comparisons of the experimental molecular constants of the $3^3\Pi_g$ and the $4^3\Sigma_g^+$ states with theoretical predictions. Note that the B_e values listed for Ref. [75] were calculated from the R_e values given in the reference using Eq. (2).

State	T_e	ω_e	B_e	
$3^3\Pi_g$	24268.404	44.2151	0.016767	This paper
	24276.5	45.6	0.01750	[76]
	24232	45.4	0.01720	[75]
$4^3\Sigma_g^+$	24294.983	47.6712	0.017335	This paper
	24 323.7	46.3	0.01800	[76]
	24313	46.7	0.01770	[75]

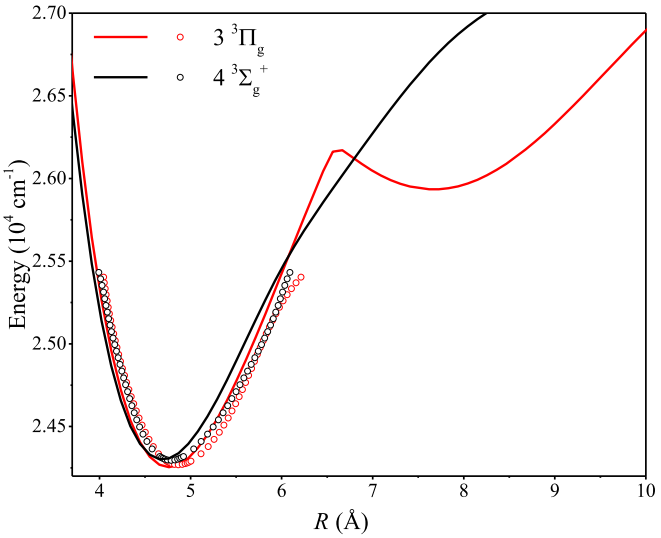

FIG. 8. Potential-energy curves of the Rb_2 $3^3\Pi_g$ and $4^3\Sigma_g^+$ electronic states. The solid lines are *ab initio* calculations from Ref. [76] and the RKR results are represented as circles.

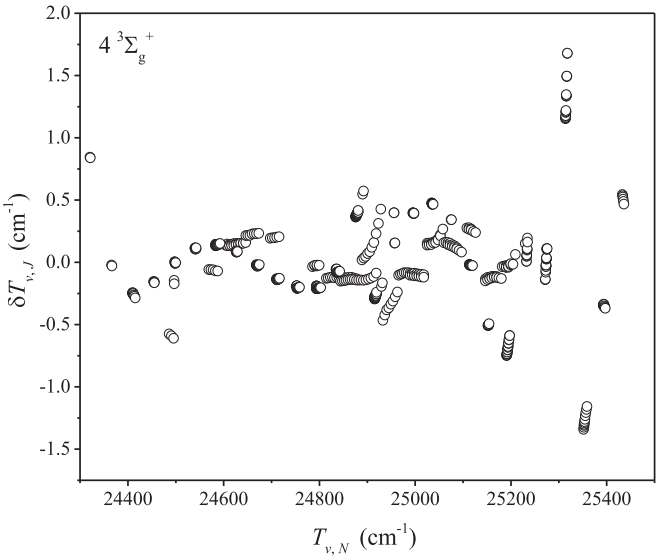

FIG. 10. Dunham expansion fit residuals of the observed $4^3\Sigma_g^+$ state rovibrational term values.

RKR curves for the $3^3\Pi_g$ state above 25 300 cm^{-1}. The theoretical calculations for $3^3\Pi_g$ predict a barrier and a secondary well. In contrast, our RKR curve in this range appears to suggest a simple broadening of the potential or the existence of a shelf.

The presence of perturbations in the observed term values is evident in the Dunham fit residuals plotted in Figs. 9 and 10 for the $3^3\Pi_g$ and $4^3\Sigma_g^+$ states, respectively. Indicative of this are the clearly observed rotational dependences of the residuals of some of the vibrational levels. This is expected for highly excited electronic states of Rb_2 due to the high density of states and the presence of various allowed nonadiabatic couplings. For both states the perturbations are enlarged above 25 300 cm^{-1}. Similar perturbation enhancement has been previously observed in the same energy region for the $3^1\Pi_g$ and $6^1\Sigma_g^+$ states [77,78]. Thus, it can be concluded that in this energy range the $3^1\Pi_g$, $6^1\Sigma_g^+$, $3^3\Pi_g$ and $4^3\Sigma_g^+$ states strongly perturb each other. The current absence of details about the interactions that cause these perturbations prevents the use of coupled-channel methods [50,63,65,114,115] for global simultaneous analysis of the perturbing states.

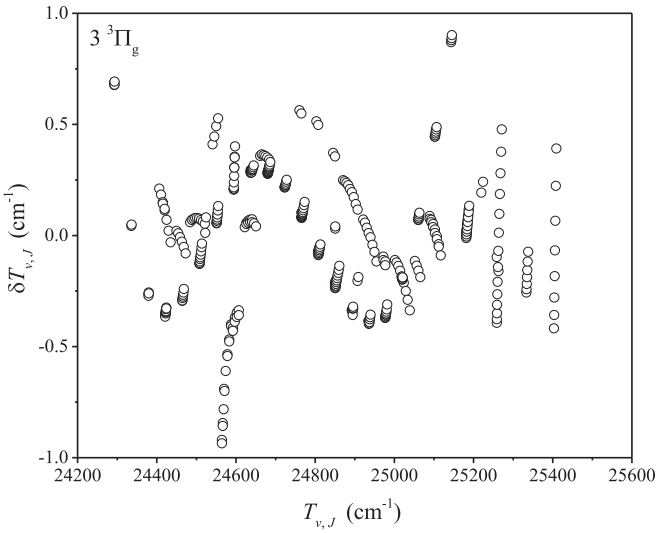

FIG. 9. Dunham expansion fit residuals of the observed $3^3\Pi_g$ state rovibrational term values.

IV. CONCLUSIONS

We have observed a large set of rovibrational levels of the $3^3\Pi_g$ and $4^3\Sigma_g^+$ states of the Rb_2 dimer using the PFOODR technique. Well-defined Condon structures were observed in the resolved bound-free fluorescence from the laser-populated upper levels to the repulsive region of the $a^3\Sigma_u^+$ state potential. This allowed us to determine the vibrational quantum number assignment of the observed states as well as to confirm their triplet character. The experimental observations reveal the presence of many perturbations in the observed energy range of the $3^3\Pi_g$ and $4^3\Sigma_g^+$ states. In addition, the strong enhancement of the perturbations around 25 300 cm^{-1} is compelling evidence for the existence of avoided crossings of potential-energy curves in this range. In spite of the irregularities in the observed data due to the presence of perturbations, we were able to construct potential curves for both states using the Dunham expansion and the RKR method.

ACKNOWLEDGMENTS

This work was supported by National Science Foundation Grant No. NSF PHY 1912269, the Lagerqvist Research Fund of Temple University, a collaborative grant of the Russian Foundation for Basic Research (RFBR) and National Natural Science Foundation of China (NSFC) (RFBR Grant No. 20-53-53025 and NSFC Grant No. 62011530047), and NSFC Grant No. 62020106014. We are grateful to Prof. John Huennekens of Lehigh University for helpful discussions on the collisional propensity rules.

[1] K. K. Ni, S. Ospelkaus, M. H. G. de Miranda, A. Pe'er, B. Neyenhuis, J. J. Zirbel, S. Kotochigova, P. S. Julienne, D. S. Jin, and J. Ye, A high phase-space-density gas of polar molecules, Science **322**, 231 (2008).

[2] W. Salzmann, U. Poschinger, R. Wester, M. Weidemuller, A. Merli, S. M. Weber, F. Sauer, M. Plewicki, F. Weise, A. M. Esparza, L. Woste, and A. Lindinger, Coherent control with shaped femtosecond laser pulses applied to ultracold molecules, Phys. Rev. A **73**, 023414 (2006).

[3] M. H. G. de Miranda, A. Chotia, B. Neyenhuis, D. Wang, G. Quemener, S. Ospelkaus, J. L. Bohn, J. Ye, and D. S. Jin, Controlling the quantum stereodynamics of ultracold bimolecular reactions, Nat. Phys. **7**, 502 (2011).

[4] T. Volz, N. Syassen, D. M. Bauer, E. Hansis, S. Durr, and G. Rempe, Preparation of a quantum state with one molecule at each site of an optical lattice, Nat. Phys. **2**, 692 (2006).

[5] J. G. Danzl, E. Haller, M. Gustavsson, M. J. Mark, R. Hart, N. Bouloufa, O. Dulieu, H. Ritsch, and H.-C. Naegerl, Quantum gas of deeply bound ground state molecules, Science **321**, 1062 (2008).

[6] T. M. Rvachov, H. Son, A. T. Sommer, S. Ebadi, J. J. Park, M. W. Zwierlein, W. Ketterle, and A. O. Jamison, Long-Lived Ultracold Molecules with Electric and Magnetic Dipole Moments, Phys. Rev. Lett. **119**, 143001 (2017).

[7] C. Gross and I. Bloch, Quantum simulations with ultracold atoms in optical lattices, Science **357**, 995 (2017).

[8] B. Yan, S. A. Moses, B. Gadway, J. P. Covey, K. R. A. Hazzard, A. M. Rey, D. S. Jin, and J. Ye, Observation of dipolar spin-exchange interactions with lattice-confined polar molecules, Nature (London) **501**, 521 (2013).

[9] P. Kusch and M. M. Hessel, An analysis of $A^1\Sigma_u^+ - X^1\Sigma_g^+$ band system of $^7Li_2$, J. Chem. Phys. **67**, 586 (1977).

[10] M. E. Koch, W. C. Stwalley, and C. B. Collins, Observation of Bound-Free-Bound Triplet Absorption-Bands in Li_2, Phys. Rev. Lett. **42**, 1052 (1979).

[11] R. A. Bernheim, L. P. Gold, P. B. Kelly, C. Tomczyk, and D. K. Veirs, A spectroscopic study of the $E^1\Sigma_g^+$ and $F^1\Sigma_g^+$ states of $^7Li_2$ by pulsed optical–optical double resonance, J. Chem. Phys. **74**, 3249 (1981).

[12] R. A. Bernheim, L. P. Gold, P. B. Kelly, T. Tipton, and D. K. Veirs, A spectroscopic study of the $G^1\Pi_g$ state of $^7Li_2$ by pulsed optical–optical double resonance, J. Chem. Phys. **74**, 2749 (1981).

[13] R. A. Bernheim, L. P. Gold, and T. Tipton, Rydberg states of $^7Li_2$ by pulsed optical–optical double resonance spectroscopy: Molecular constants of $^7Li_2^+$, J. Chem. Phys. **78**, 3635 (1983).

[14] X. B. Xie and R. W. Field, The $^6Li_2$ $A^1\Sigma_u^+ \sim b^3\Pi_u$ Spin-orbit perturbations: Sub-doppler spectra and steady-state kinetic lineshape model, Chem. Phys. **99**, 337 (1985).

[15] B. Barakat, R. Bacis, F. Carrot, S. Churassy, P. Crozet, F. Martin, and J. Verges, Extensive analysis of the $X^1\Sigma_g^+$ ground state of $^7Li_2$ by laser-induced fluorescence Fourier transform spectrometry, Chem. Phys. **102**, 215 (1986).

[16] R. A. Bernheim, L. P. Gold, C. A. Tomczyk, and C. R. Vidal, Spectroscopic study of the $E^1\Sigma_g^+$ "shelf" state in $^7Li_2$, J. Chem. Phys. **87**, 861 (1987).

[17] L. Li, T. An, T. J. Whang, A. M. Lyyra, W. C. Stwalley, R. W. Field, and R. A. Bernheim, Hyperfine Splitting of the $1^3\Delta_g$ Rydberg State of $^7Li_2$, J. Chem. Phys. **96**, 3342 (1992).

[18] A. Yiannopoulou, K. Urbanski, A. M. Lyyra, L. Li, B. Ji, J. T. Bahns, and W. C. Stwalley, Perturbation Facilitated Optical-Optical Double-Resonance Spectroscopy of the $2^3\Sigma_g^+$, $3^3\Sigma_g^+$, and $4^3\Sigma_g^+$ Rydberg States of $^7Li_2$, J. Chem. Phys. **102**, 3024 (1995).

[19] K. Urbanski, S. Antonova, A. Yiannopoulou, A. M. Lyyra, and W. C. Stwalley, All optical triple resonance spectroscopy of the $A^1\Sigma_u^+$ state of $^7Li_2$, J. Chem. Phys. **104**, 2813 (1996).

[20] L. Li and A. M. Lyyra, Triplet states of Na_2 and Li_2 by perturbation facilitated optical-optical double resonance spectroscopy, Spectrochim. Acta, Part A **55**, 2147 (1999).

[21] S. Antonova, G. Lazarov, K. Urbanski, A. M. Lyyra, L. Li, G. H. Jeung, and W. C. Stwalley, Predissociation of the $F(4)^1\Sigma_g^+$ state of Li_2, J. Chem. Phys. **112**, 7080 (2000).

[22] W. Jastrzebski, A. Pashov, and P. Kowalczyk, The $E^1\Sigma_g^+$ state of lithium dimer revised, J. Chem. Phys. **114**, 10725 (2001).

[23] P. Yi, M. Song, Y. M. Liu, A. M. Lyyra, and L. Li, New pair of $A^1\Sigma_u^+ \sim b^3\Pi_u$ mixed levels in Li_6Li_7, Chem. Phys. Lett. **349**, 426 (2001).

[24] P. Kusch and M. M. Hessel, An analysis of the $B^1\Pi_u$ -$X^1\Sigma_g^+$ band system of Na_2, J. Chem. Phys. **68**, 2591 (1978).

[25] L. Li and R. W. Field, Direct observation of high-lying $^3\Pi_g$ states of the sodium molecule by optical-optical double resonance, J. Phys. Chem. **87**, 3020 (1983).

[26] O. Babaky and K. Hussein, The ground state $X^1\Sigma_g^+$ of Na_2, Can. J. Phys. **67**, 912 (1989).

[27] L. Li, Q. S. Zhu, and R. W. Field, The Hyperfine-Structure of the Na_2 $4^3\Sigma_g^+$ State, Mol. Phys. **66**, 685 (1989).

[28] C. C. Tsai, J. T. Bahns, T. J. Whang, H. Wang, W. C. Stwalley, and A. M. Lyyra, Optical-Optical Double Resonance Spectroscopy of the $^1\Sigma_g^+$ "Shelf" States and $^1\Pi_g$ States of Na_2 Using an Ultrasensitive Ionization Detector, Phys. Rev. Lett. **71**, 1152 (1993).

[29] C. C. Tsai, T. J. Whang, J. T. Bahns, and W. C. Stwalley, The $3^1\Sigma_g^+$ "shelf" state of Na_2, J. Chem. Phys. **99**, 8480 (1993).

[30] C. C. Tsai, J. T. Bahns, and W. C. Stwalley, Optical–optical double resonance spectroscopy of the $5^1\Sigma_g^+$ "shelf" state of Na_2 using an ultrasensitive ionization detector, J. Chem. Phys. **100**, 768 (1994).

[31] C. C. Tsai, J. T. Bahns, H. Wang, T. J. Whang, and W. C. Stwalley, Optical–optical double resonance spectroscopy of the $4^1\Sigma_g^+$ "shelf" state of Na_2 using an ultrasensitive ionization detector, J. Chem. Phys. **101**, 25 (1994).

[32] T. Laue, P. Pellegrini, O. Dulieu, C. Samuelis, H. Knockel, F. Masnou-Seeuws, and E. Tiemann, Observation of the long-range potential well of the $(6)^1\Sigma_g^+(3s+5s)$ state of Na_2, European Physical Journal D **26**, 173 (2003).

[33] Y. M. Liu, L. Li, G. Lazarov, A. Lazoudis, A. M. Lyyra, and R. W. Field, Hyperfine structures of the $2^3\Sigma_g^+$, $3^3\Sigma_g^+$, and $4^3\Sigma_g^+$ states of Na_2, J. Chem. Phys. **121**, 5821 (2004).

[34] L. Li, A. M. Lyyra, W. T. Luh, and W. C. Stwalley, Observation of the $^{39}K_2$ $a^3\Sigma_u^+$ state by perturbation facilitated optical–optical double resonance resolved fluorescence spectroscopy, J. Chem. Phys. **93**, 8452 (1990).

[35] C. Amiot, J. Verges, and C. E. Fellows, The long-range potential of the K_2 $X^1\Sigma_g^+$ ground electronic state up to 15 Å, J. Chem. Phys. **103**, 3350 (1995).

[36] J. T. Kim, H. Wang, C. C. Tsai, J. T. Bahns, W. C. Stwalley, G. Jong, and A. M. Lyyra, Observation of the $4^3\Sigma_g^+$, $3^3\Pi_g$, $2^3\Delta_g$, and $b^3\Pi_u$ states of $^{39}K_2$ by perturbation facilitated

optical–optical double resonance spectroscopy, J. Chem. Phys. **102**, 6646 (1995).

[37] M. R. Manaa, A. J. Ross, F. Martin, P. Crozet, A. M. Lyyra, L. Li, C. Amiot, and T. Bergeman, Spin-orbit interactions, new spectral data, and deperturbation of the coupled $b^3\Pi_u$ and $A^1\Sigma_u^+$ states of K_2, J. Chem. Phys. **117**, 11208 (2002).

[38] J. Magnes, E. Ahmed, C. Goldberg, A. M. Lyyra, S. Magnier, M. Aubert-Frecon, Y. M. Liu, and L. Li, Observation of the K_2 $4^3\Delta_g$ state by cw perturbation-facilitated optical-optical double resonance spectroscopy, J. Mol. Spectrosc. **221**, 72 (2003).

[39] E. Ahmed, A. M. Lyyra, F. Xie, D. Li, Y. Chu, L. Li, V. S. Ivanov, V. B. Sovkov, and S. Magnier, New experimental data on the K_2 $a^3\Sigma_u^+$ state analyzed with the multi-parameter approach, J. Mol. Spectrosc. **234**, 41 (2005).

[40] Y. Chu, F. Xie, D. Li, L. Li, V. B. Sovkov, V. S. Ivanov, and A. M. Lyyra, Experimental study of the $^{39}K_2$ $2^3\Pi_g$ state by perturbation facilitated infrared-infrared double resonance and two-photon excitation spectroscopy, J. Chem. Phys. **122**, 074302 (2005).

[41] F. Xie, D. Li, L. Li, R. W. Field, and S. Magnier, Infrared-Infrared double resonance spectroscopy of $^{39}K_2$: The $1^3\Delta_g$ state, Chem. Phys. Lett. **431**, 267 (2006).

[42] S. Falke, I. Sherstov, E. Tiemann, and C. Lisdat, The $A^1\Sigma_u^+$ state of K_2 up to the dissociation limit, J. Chem. Phys. **125**, 224303 (2006).

[43] D. Li, F. Xie, L. Li, V. B. Sovkov, V. S. Ivanov, E. Ahmed, A. M. Lyyra, J. Huennekens, and S. Magnier, The $^{39}K_2$ $2^3\Sigma_g^+$ state: Observation and analysis, J. Chem. Phys. **126**, 194314 (2007).

[44] A. Pashov, P. Popov, H. Knockel, and E. Tiemann, Spectroscopy of the $a^3\Sigma_u^+$ state and the coupling to the $X\,^1\Sigma_g^+$ state of K_2, Eur. Phys. J. D **46**, 241 (2008).

[45] C. Amiot and T. S. Carter, Laser-induced fluorescence of Rb_2: The $(1)^1\Sigma_g^+(X)$, $(2)^1\Sigma_g^+$, $(1)^1\Pi_u(B)$, $(1)^1\Pi_g$, and $(2)^1\Pi_u(C)$ electronic states, J. Chem. Phys. **93**, 8591 (1990).

[46] J. D. Miller, R. A. Cline, and D. J. Heinzen, Photoassociation Spectrum of Ultracold Rb Atoms, Phys. Rev. Lett. **71**, 2204 (1993).

[47] C. Amiot and J. Vergès, Optical-optical double resonance and Fourier transform spectroscopy: The Rb_2 $B^1\Pi_u$ electronic state up to the quasibound energy levels, Chem. Phys. Lett. **274**, 91 (1997).

[48] C. Amiot, O. Dulieu, and J. Vergès, Resolution of the Apparent Disorder of the Rb_2 $A^1\Sigma_u^+(0_u^+)$ and $b^3\Pi_u(0_u^+)$ Spectra: A Case of Fully Coupled Electronic States, Phys. Rev. Lett. **83**, 2316 (1999).

[49] J. Y. Seto, R. J. Le Roy, J. Verges, and C. Amiot, Direct potential fit analysis of the $X^1\Sigma_g^+$ state of Rb_2: Nothing else will do!, J. Chem. Phys. **113**, 3067 (2000).

[50] H. Salami, T. Bergeman, B. Beser, J. Bai, E. H. Ahmed, S. Kotochigova, A. M. Lyyra, J. Huennekens, C. Lisdat, A. V. Stolyarov, O. Dulieu, P. Crozet, and A. J. Ross, Spectroscopic observations, spin-orbit functions, and coupled-channel deperturbation analysis of data on the $A^1\Sigma_u^+$ and $b^3\Pi_u$ states of Rb_2, Phys. Rev. A **80**, 022515 (2009).

[51] B. Beser, V. B. Sovkov, J. Bai, E. H. Ahmed, C. C. Tsai, F. Xie, L. Li, V. S. Ivanov, and A. M. Lyyra, Experimental investigation of the $^{85}Rb_2$ $a^3\Sigma_u^+$ triplet ground state: Multiparameter Morse long range potential analysis, J. Chem. Phys. **131**, 094505 (2009).

[52] Y. Guan, X. Han, J. Yang, Z. Zhou, X. Dai, E. H. Ahmed, A. M. Lyyra, S. Magnier, V. S. Ivanov, A. S. Skublov, and V. B. Sovkov, Updated potential energy function of the Rb_2 $a^3\Sigma_u^+$ state in the attractive and repulsive regions determined from its joint analysis with the $2^3\Pi_{0g}$ state, J. Chem. Phys. **139**, 144303 (2013).

[53] A. N. Drozdova, A. V. Stolyarov, M. Tamanis, R. Ferber, P. Crozet, and A. J. Ross, Fourier transform spectroscopy and extended deperturbation treatment of the spin-orbit-coupled $A^1\Sigma_u^+$ and $b^3\Pi_u$ states of the Rb_2 molecule, Phys. Rev. A **88**, 022504 (2013).

[54] X. Han, J. Yang, Y. Guan, Z. Zhou, W. Zhao, A. R. Allouche, S. Magnier, E. H. Ahmed, A. M. Lyyra, and X. Dai, Observation of the $4^1\Sigma_g^+$ State of Rb_2, Chem. Phys. Lett. **601**, 124 (2014).

[55] I. Havalyova, A. Pashov, P. Kowalczyk, J. Szczepkowski, and W. Jastrzebski, The coupled system of $(5)^1\Sigma_u^+$ and $(5)^1\Pi_u$ electronic states in Rb_2, J. Quant. Spectrosc. Radiat. Transfer **202**, 328 (2017).

[56] A. Pashov, P. Kowalczyk, A. Grochola, J. Szczepkowski, and W. Jastrzebski, Coupled-channels analysis of the ($5^1\Sigma_u^+$, $5^1\Pi_u$, $5^3\Pi_u$, $2^3\Delta_u$) complex of electronic states in rubidium dimer, J. Quant. Spectrosc. Radiat. Transfer **221**, 225 (2018).

[57] A. Pashov, P. Kowalczyk, and W. Jastrzebski, Double-minimum $3^1\Sigma_u^+$ state in Rb_2: Spectroscopic study and possible applications for cold-physics experiments, Phys. Rev. A **100**, 012507 (2019).

[58] C. Amiot and O. Dulieu, The Cs_2 ground electronic state by Fourier transform spectroscopy: Dispersion coefficients, J. Chem. Phys. **117**, 5155 (2002).

[59] F. Xie, V. B. Sovkov, A. M. Lyyra, D. Li, S. Ingram, J. Bai, V. S. Ivanov, S. Magnier, and L. Li, Experimental investigation of the Cs_2 $a^3\Sigma_u^+$ triplet ground state: Multiparameter Morse long range potential analysis and molecular constants, J. Chem. Phys. **130**, 051102 (2009).

[60] J. A. Coxon and P. G. Hajigeorgiou, The ground $X^1\Sigma_g^+$ electronic state of the cesium dimer: Application of a direct potential fitting procedure, J. Chem. Phys. **132**, 094105 (2010).

[61] F. Xie, L. Li, D. Li, V. B. Sovkov, K. V. Minaev, V. S. Ivanov, A. M. Lyyra, and S. Magnier, Joint analysis of the Cs_2 $a^3\Sigma_u^+$ and 1_g $3^3\Pi_{1g}$ states, J. Chem. Phys. **135**, 024303 (2011).

[62] S. Sainis, J. Sage, E. Tiesinga, S. Kotochigova, T. Bergeman, and D. DeMille, Detailed spectroscopy of the Cs_2 $a^3\Sigma_u^+$ state and implications for measurements sensitive to variation of the electron-proton mass ratio, Phys. Rev. A **86**, 022513 (2012).

[63] A. Znotins, A. Kruzins, M. Tamanis, R. Ferber, E. A. Pazyuk, A. V. Stolyarov, and A. Zaitsevskii, Fourier-transform spectroscopy, relativistic electronic structure calculation, and coupled-channel deperturbation analysis of the fully mixed $A^1\Sigma_u^+$ and $b^3\Pi_u$ states of Cs_2, Phys. Rev. A **100**, 042507 (2019).

[64] V. B. Sovkov, F. Xie, A. M. Lyyra, E. H. Ahmed, J. Ma, and S. Jia, Re-examination of the Cs_2 ground singlet $X^1\Sigma_g^+$ and triplet $a^3\Sigma_u^+$ states, J. Chem. Phys. **147**, 104301 (2017).

[65] J. Bai, E. H. Ahmed, B. Beser, Y. Guan, S. Kotochigova, A. M. Lyyra, S. Ashman, C. M. Wolfe, J. Huennekens, F. Xie, D. Li,

L. Li, M. Tamanis, R. Ferber, A. Drozdova, E. Pazyuk, A. V. Stolyarov, J. G. Danzl, H. C. Nägerl, N. Bouloufa, O. Dulieu, C. Amiot, H. Salami, and T. Bergeman, Global analysis of data on the spin-orbit-coupled $A^1\Sigma_u^+$ and $b^3\Pi_u$ states of Cs_2, Phys. Rev. A **83**, 032514 (2011).

[66] H. Partridge, D. A. Dixon, S. P. Walch, C. W. Bauschlicher, and J. L. Gole, Electron affinities of the alkali dimers: Na_2, K_2, and Rb_2, J. Chem. Phys. **79**, 1859 (1983).

[67] B. Bussery and M. Aubertfrecon, Multipolar long-range electrostatic, dispersion, and induction energy terms for the interactions between 2 identical alkali atoms Li, Na, K, Rb, and Cs in various electronic states, J. Chem. Phys. **82**, 3224 (1985).

[68] F. Spiegelmann, D. Pavolini, and J. P. Daudey, Theoretical study of the excited states of the heavier alkali dimers. II. The Rb_2 molecule, J. Phys. B **22**, 2465 (1989).

[69] M. Krauss and W. J. Stevens, Effective Core Potentials and Accurate Energy Curves For Cs_2 and other Alkali Diatomics, J. Chem. Phys. **93**, 4236 (1990).

[70] M. Foucrault, P. Millie, and J. P. Daudey, Nonperturbative method for core valence correlation in pseudopotential calculations - application to the Rb_2 and Cs_2 molecules, J. Chem. Phys. **96**, 1257 (1992).

[71] S. Kotochigova, E. Tiesinga, and P. S. Julienne, Relativistic *ab initio* treatment of the second-order spin-orbit splitting of the $a^3\Sigma_u^+$ potential of rubidium and cesium dimers, Phys. Rev. A **63**, 012517 (2000).

[72] S. J. Park, S. W. Suh, Y. S. Lee, and G. H. Jeung, Theoretical study of the electronic states of the Rb_2 molecule, J. Mol. Spectrosc. **207**, 129 (2001).

[73] A. A. Khuskivadze, M. I. Chibisov, and I. I. Fabrikant, Adiabatic energy levels and electric dipole moments of Rydberg states of Rb_2 and Cs_2 dimers, Phys. Rev. A **66**, 042709 (2002).

[74] D. Edvardsson, S. Lunell, and C. M. Marian, Calculation of potential energy curves for Rb_2 including relativistic effects, Mol. Phys. **101**, 2381 (2003).

[75] M. Tomza, W. Skomorowski, M. Musial, R. Gonzalez-Ferez, C. P. Koch, and R. Moszynski, Interatomic potentials, electric properties and spectroscopy of the ground and excited states of the Rb_2 molecule: *Ab initio* calculations and effect of a non-resonant field, Mol. Phys. **111**, 1781 (2013).

[76] W. Jastrzebski, P. Kowalczyk, J. Szczepkowski, A. R. Allouche, P. Crozet, and A. J. Ross, High-lying electronic states of the rubidium dimer *ab initio* predictions and experimental observation of the $5^1\Sigma_u^+$ and $5^1\Pi_u$ states of Rb_2 by polarization labelling spectroscopy, J. Chem. Phys. **143**, 044308 (2015).

[77] P. T. Arndt, V. B. Sovkov, J. Ma, X. H. Pan, D. S. Beecher, J. Y. Tsai, Y. F. Guan, A. M. Lyyra, and E. H. Ahmed, The Rb_2 $3^1\Pi_g$ state: Observation and analysis, J. Chem. Phys. **149**, 224303 (2018).

[78] P. T. Arndt, V. B. Sovkov, J. Ma, X. H. Pan, D. S. Beecher, J. Y. Tsai, Y. F. Guan, A. M. Lyyra, and E. H. Ahmed, Experimental study of the $6^1\Sigma_g^+$ state of the rubidium dimer, Phys. Rev. A **99**, 052511 (2019).

[79] J. R. d. Laeter, J. K. Böhlke, P. D. Bièvre, H. Hidaka, H. S. Peiser, K. J. R. Rosman, and P. D. P. Taylor, Atomic weights of the elements. Review 2000 (IUPAC Technical Report), Pure Appl. Chem. **75**, 683 (2003).

[80] C. R. Vidal and J. Cooper, Heat-pipe oven - a new, well-defined metal vapor device for spectroscopic measurements, J. Appl. Phys. **40**, 3370 (1969).

[81] A. N. Nesmeyanov, *Vapor Pressure of the Chemical Elements* (Elsevier, Amsterdam, 1963).

[82] W. Demtröder, *Laser Spectroscopy: Basic Concepts and Instrumentation* (Springer, New York, 2003).

[83] J. E. Sansonetti, Wavelengths, transition probabilities, and energy levels for the spectra of rubidium (RbI through RbXXXVII), J. Phys. Chem. Ref. Data **35**, 301 (2006).

[84] X. B. Xie and R. W. Field, Perturbation Facilitated Optical-Optical Double Resonance spectroscopy of the $^6Li_2$ $3^3\Sigma_g$, $2^3\Pi_g$, $1^3\Delta_g$, $b^3\Pi_u$, and $a^3\Sigma_u^+$ state, J. Mol. Spectrosc. **117**, 228 (1986).

[85] B. A. Palmer, R. A. Keller, and R. Engleman, *An Atlas of Uranium Emission Intensities in a Hollow Cathode Discharge* (Los Alamos Scientific Laboratory, Los Alamos, NM, 1980).

[86] R. A. Keller, R. Engleman, and B. A. Palmer, Atlas for optogalvanic wavelength calibration, Appl. Opt. **19**, 836 (1980).

[87] P. F. Bernath, *Spectra of Atoms and Molecules* (Oxford University, New York, 2005).

[88] S. Gerstenkorn and P. Luc, *Atlas of the Absorption Spectra of Molecular Iodine for* $14,800\,cm^{-1}$ *to* $20,000\,cm^{-1}$ (CNRS, Paris, 1978).

[89] S. Gerstenkorn and P. Luc, Absolute iodine I_2 standards measured by means of fourier-transform spectroscopy, Rev. Phys. Appl. **14**, 791 (1979).

[90] E. J. Breford and F. Engelke, Laser-induced molecular fluorescence in supersonic nozzle beams: Applications to the NaK $D^1\Pi_u^+ - X^1\Sigma^+$ and $D^1\Pi_u^+ - a^3\Sigma^+$ systems, Chem. Phys. Lett. **53**, 282 (1978).

[91] E. U. Condon, Nuclear motions associated with electron transitions in diatomic molecules, Phys. Rev. **32**, 858 (1928).

[92] G. Herzberg, *Spectra of Diatomic Molecules* (Van Nostrand, New York, 1950).

[93] J. X. Yang, W. Zhao, X. H. Pan, H. M. Wei, J. Ma, E. H. Ahmed, A. M. Lyyra, and X. C. Dai, Experimental study of the $b^3\Pi_{1u}$ and $2^3\Pi_{1g}$ states of $^{85}Rb_2$, J. Mol. Spectrosc. **336**, 36 (2017).

[94] L. Li, Q. S. Zhu, A. M. Lyyra, T. J. Whang, W. C. Stwalley, R. W. Field, and M. H. Alexander, Collision-Induced Transitions between $A^1\Sigma_u^+$ and $b^3\Pi_u$ states of Na_2 - the gateway effect of perturbed levels, J. Chem. Phys. **97**, 8835 (1992).

[95] Y. Gao, P. S. Gorgone, S. Davis, E. K. McCall, and B. Stewart, Dependence of level-resolved energy transfer on initial vibrational level in Li_2 $A^1\Sigma_u^+$–Ne collisions, J. Chem. Phys. **104**, 1415 (1996).

[96] L. Li, S. Antonova, A. Yiannopoulou, K. Urbanski, and A. M. Lyyra, State-to-state collision energy transfer of $^7Li_2$ within high-lying triplet states: Gateway effect of mixed levels in energy transfer between singlet and triplet states, J. Chem. Phys. **105**, 9859 (1996).

[97] C. Ottinger, R. Velasco, and R. N. Zare, Some Propensity Rules in Collision-Induced Rotational Quantum Jumps, J. Chem. Phys. **52**, 1636 (1970).

[98] See Supplemental Material at http://link.aps.org/supplemental/10.1103/PhysRevA.105.032823 for the experimental term values, bound-free spectra, and RKR

potential functions of the Rb_2 $3^3\Pi_g$ and $4^3\Sigma_g^+$ electronic states.

[99] Vladimir B. Sovkov and J. Ma, in *Advances in Computer Science Research: Proceedings of the 2016 International Conference on Applied Mathematics, Simulation and Modelling* (Atlantis, Beijing, 2016), p. 369.

[100] V. B. Sovkov, in Optimizer: Source Codes and Manuals and Collection of Applications available at https://sourceforge.net/projects/optimizer-sovkov/.

[101] S. S. Onishchenko, V. B. Sovkov, F. Xie, D. Li, S. S. Lukashov, V. V. Baturo, J. Wu, J. Ma, and L. Li, Analysis of the hyperfine structure of the Cs_2 $3^3\Sigma_g^+$ state, J. Quant. Spectrosc. Radiat. Transfer **250**, 107037 (2020).

[102] X. Wang, W. Liu, Y. Li, J. Wu, V. B. Sovkov, J. Ma, S. Onishchenko, P. Li, Y. Fu, D. Li, Q. Fan, L. Xiao, and S. Jia, Hyperfine structure of the NaCs $b^3\Pi_2$ state near the dissociation limit $3S_{1/2} + 6P_{3/2}$ observed with ultracold atomic photoassociation, Phys. Chem. Chem. Phys. **22**, 3809 (2020).

[103] S. S. Onishchenko, V. B. Sovkov, F. Xie, D. Li, S. S. Lukashov, V. V. Baturo, J. Wu, and J. Ma, Analysis of the hyperfine structure of the $1^3\Delta_g$, $2^3\Pi_g$, and $3^3\Sigma_g^+$ states of $^6Li^7Li$, J. Quant. Spectrosc. Radiat. Transfer **270**, 107665 (2021).

[104] J. L. Dunham, The energy levels of a rotating vibrator, Phys. Rev. **41**, 721 (1932).

[105] R. Rydberg, Graphical Representation of some bound spectroscopic Results, Z. Phys. **73**, 376 (1932).

[106] R. Rydberg, Some potential curves of mercury hydrides, Z. Phys. **80**, 514 (1933).

[107] O. Klein, For the calculation of potential curves for diatomic molecules with spectral help, Z. Phys. **76**, 226 (1932).

[108] A. L. G. Rees, The calculation of potential-energy curves from band-spectroscopic data, Proc. Phys. Soc. London **59**, 998 (1947).

[109] J. Tellinghuisen, A direct potential fitting RKR method: Semiclassical vs. quantal comparisons, J. Mol. Spectrosc. **330**, 20 (2016).

[110] E. W. Kaiser, Dipole moment and hyperfine parameters of $H^{35}Cl$ and $D^{35}Cl$, J. Chem. Phys. **53**, 1686 (1970).

[111] A. W. Mantz, J. K. G. Watson, K. N. Rao, D. L. Albritton, A. L. Schmeltekopf, and R. N. Zare, Rydberg-Klein-Rees potential for the $X^1\Sigma^+$ state of the CO molecule, J. Mol. Spectrosc. **39**, 180 (1971).

[112] J. K. G. Watson, The isotope dependence of diatomic Dunham coefficients, J. Mol. Spectrosc. **80**, 411 (1980).

[113] V. G. Tyuterev and T. I. Velichko, High-order anharmonicity parameters in various representations of the diatomic potential function and exact relations between spectroscopic constants. application to the co molecule, Chem. Phys. Lett. **104**, 596 (1984).

[114] P. Qi, J. Bai, E. Ahmed, A. M. Lyyra, S. Kotochigova, A. J. Ross, C. Effantin, P. Zalicki, J. Vigue, G. Chawla, R. W. Field, T. J. Whang, W. C. Stwalley, H. Knockel, E. Tiemann, J. Shang, L. Li, and T. Bergeman, New spectroscopic data, spin-orbit functions, and global analysis of data on the $A^1\Sigma_u^+$ and $b^3\Pi_u$ states of Na_2, J. Chem. Phys. **127**, 044301 (2007).

[115] J. Zaharova, M. Tamanis, R. Ferber, A. N. Drozdova, E. A. Pazyuk, and A. V. Stolyarov, Solution of the fully-mixed-state problem: Direct deperturbation analysis of the $A^1\Sigma^+$ -$b^3\Pi$ complex in a NaCs dimer, Phys. Rev. A **79**, 012508 (2009).